

# Axial and Equatorial Hydrogen-Bond Conformers and Ring-Puckering Motion in the Trimethylene Sulfide · Hydrogen Fluoride Complex

M. Eugenia Sanz, Juan C. López, and José L. Alonso\*<sup>[a]</sup>

**Abstract:** Axial and equatorial hydrogen-bond conformers of the trimethylene sulfide...hydrogen fluoride complex have been generated and characterized in the supersonic jet of a molecular beam Fourier transform microwave experiment. It is shown that the ring-puckering large amplitude motion of trimethylene sulfide is responsible for the observed conformers. The axial conformer has been found to be the most stable and has been proved by the existence of relaxation of the high-energy equatorial form to it. This con-

formational preference has been explained in the context of a delicate balance between primary and secondary hydrogen bonds. The interconversion between both conformers takes place through the ring-puckering motion of the heterocycle, provided that the barrier to the ring inversion remains low after complexation, as all experimental

findings indicate. The structural parameters of the trimethylene sulfide and the hydrogen bond have been derived from the analysis of the rotational spectra of the  $\text{C}_3\text{H}_6^{32}\text{S}\cdots\text{HF}$ ,  $\text{C}_3\text{H}_6^{34}\text{S}\cdots\text{HF}$ ,  $^{13}\text{C}_\alpha^{12}\text{C}_\beta^{12}\text{H}_6^{32}\text{S}\cdots\text{HF}$ , and  $^{13}\text{C}_\beta^{12}\text{C}_\alpha^{12}\text{H}_6^{32}\text{S}\cdots\text{HF}$  isotopomers. Both conformers have  $C_s$  symmetry with the hydrogen fluoride located in the molecular symmetry plane of trimethylene sulfide, which is puckered at a similar angle to that found for the bare ring.

**Keywords:** hydrogen bonds · rotational spectroscopy · supersonic jets

## Introduction

Investigations of hydrogen-bond complexes by means of different spectroscopic techniques have provided a large amount of information on this topic. Nevertheless, in spite of the huge number of molecular complexes studied, little attention has been paid to the study of the conformational behaviour of the hydrogen bonding. The detection and characterization of different hydrogen-bond conformers provide valuable information about the factors which govern molecular clustering to particular binding sites in the acceptor molecule.

We have recently dealt with a systematic study of dimers which are expected to present both axial and equatorial conformers. The low-temperature environment of a supersonic jet expansion constitutes an excellent experiment to generate possible conformers which can be proved by Fourier transform microwave spectroscopy. The rotational spectra of the conformers are then obtained, from which the moments of inertia used to determine their structures can be extracted.

The resolution achieved with molecular beam Fourier transform microwave spectroscopy (MB-FTMW)<sup>[1]</sup> is such that even fairly small differences in the structures of the conformers will result in well separated spectra. Using this technique we have detected for the first time axial and equatorial conformers in the prototypical complexes of tetrahydropyran and pentamethylene sulfide with HX (X = F, Cl).<sup>[2–5]</sup> Both six-membered rings present two nonbonding electron pairs at the O or S atoms that turn out to be nonequivalent due to the chair conformations of the ring. Thus, when complexed with HX the two nonequivalent binding sites at the axial and equatorial positions led to two different axial and equatorial conformers (see Figure 1 in ref. [2]). Nevertheless, only one conformer has been observed in the studies performed for the related complexes of tetrahydrofuran and tetrahydrothiophene with HX,<sup>[6–9]</sup> since both five-membered rings exhibit a twisted-like equilibrium configuration with two equivalent nonbonding electron pairs at the heteroatom.

The role which a large amplitude motion in the acceptor molecule plays in the conformational behaviour of the hydrogen bonding has also been analysed.<sup>[10–12]</sup> To this end, the ring-puckering motion of the four-membered rings trimethylene oxide (TMO, oxetane,  $\text{C}_3\text{H}_6\text{O}$ ) and trimethylene sulfide (TMS, thietane,  $\text{C}_3\text{H}_6\text{S}$ ) is an excellent benchmark. Oxetane undergoes a ring-puckering large amplitude motion described by a double-minimum potential function with a

[a] Prof. J. L. Alonso, Dr. M. E. Sanz, Prof. J. C. López  
Departamento de Química Física  
Facultad de Ciencias, Universidad de Valladolid  
47005 Valladolid (Spain)  
Fax: (+34)-983-423264  
E-mail: jlalonso@qf.uva.es

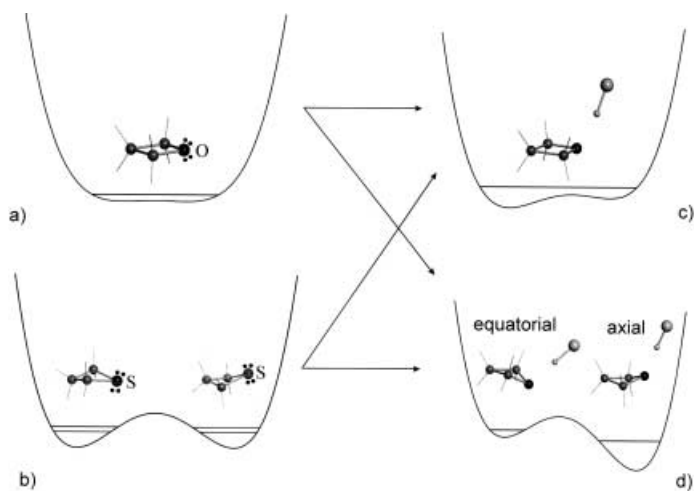


Figure 1. Ring-puckering potential functions for a) oxetane (TMO), b) thietane (TMS), c) and d) TMO and TMS complexes with HX.

barrier to the planar configuration of  $\approx 15 \text{ cm}^{-1}$ <sup>[13]</sup> (see Figure 1a). Its equilibrium conformation is effectively planar since the ground vibrational state is  $\approx 12 \text{ cm}^{-1}$  above the barrier, so that the nonbonding electron pairs at the O atom are equivalent. When complexed with HX (X = F, Cl) two different behaviours can be predicted. According to Figure 1c, if the nearly planar ring configuration is not altered upon complexation, only one conformer will be observed for the complex as the nonbonding electron pairs remain equivalent. In contrast, if complexation induces a puckered conformation in the ring (increasing sufficiently the barrier to planarity), the equivalence of the nonbonding electron pairs is broken and two different axial and equatorial conformers will appear as shown in Figure 1d. Investigation of the oxetane...HX complexes<sup>[10, 11]</sup> proved conclusively the planarity of the

oxetane ring after dimerization as only one conformer was observed for each complex. In the case of trimethylene sulfide, the ring executes a ring-puckering motion with an intermediate barrier to the planar configuration of  $274 \text{ cm}^{-1}$ .<sup>[14, 15]</sup> The tunneling effect interconverts the two  $C_s$  puckered conformations making equivalent the nonbonding electron pairs at the S atom, as shown in Figure 1b. If complexation with HX perturbs the large amplitude motion resulting in a planar or nearly planar ring, only one conformer would be expected (see Figure 1c). On the contrary, if the double minimum survives after the hydrogen bond is formed, the equivalence of the acceptor sites in the TMS monomer ends by the effect of complexation, giving rise to axial and equatorial conformers sited in the asymmetric double-minimum potential function of Figure 1d. This behaviour has been observed for the first time in our recent study of  $\text{TMS} \cdots \text{HCl}$  complex;<sup>[12]</sup> two structurally different axial and equatorial species were characterized in the supersonic expansion, the axial conformer being the most stable one.

Continuing with this investigation, we now report the experimental study of the  $\text{TMS} \cdots \text{HF}$  complex. The observation of both axial and equatorial conformers formed in the supersonic expansion constitutes a decisive piece of evidence to establish the importance that the ring-puckering large amplitude motion has in the conformational behaviour of the hydrogen bond.

**Rotational spectra:** The prediction of the rotational spectra for the axial and equatorial rotamers of the complex was done considering the structural models of Figure 1d and assuming that the structures of the  $\text{HF}$ <sup>[16]</sup> and  $\text{TMS}$ <sup>[17]</sup> monomers remain unchanged after complexation. The HF subunit was situated in the molecular symmetry plane of TMS. For the structural parameters of the hydrogen bond were adopted those of the related pentamethylene sulfide...HF and thiirane...HF complexes.<sup>[5, 18]</sup> Both conformers were then predicted to be near-prolate tops, with their rotational spectra composed of fairly intense  $\mu_a$ - and weak  $\mu_b$ -type transitions.

Using He as carrier gas, wide frequency scans were performed. Groups of  $\mu_a$ -type R-branch lines separated approximately 4600 MHz were identified as belonging to the axial form of the  $\text{TMS} \cdots \text{HF}$  complex. On the basis of these assignments, several of the much weaker  $\mu_b$ -type R- and Q-branch transitions were also identified and measured. Apart from the systematic Doppler doublet, splittings arising from the nuclear spin (H)–nuclear spin (F) interaction within the HF subunit have been observed in some of the rotational transitions, as shown in Figure 2. This interaction couples the resulting  $\mathbf{I} = \mathbf{I}_H + \mathbf{I}_F$  angular momentum with the overall rotational angular momentum  $\mathbf{J}$  to give the total angular momentum  $\mathbf{F} = \mathbf{I} + \mathbf{J}$ .

Following the same procedure,  $\mu_a$ -type R-branch spectra corresponding to the  $^{12}\text{C}_3\text{H}_6^{34}\text{S} \cdots \text{HF}$ ,  $^{13}\text{C}_\alpha^{12}\text{C}_2\text{H}_6^{32}\text{S} \cdots \text{HF}$  and  $^{13}\text{C}_\beta^{12}\text{C}_2\text{H}_6^{32}\text{S} \cdots \text{HF}$  isotopomers were detected in their natural abundances. All the transitions measured, along with their assignments, are listed in Table 1. When the nuclear spin (H)–nuclear spin (F) hyperfine structure was not resolved, the observed frequency was assigned to the quantum label of the strongest component.

**Abstract in Spanish:** Los conformeros axial y ecuatorial del complejo formado por sulfuro de trimetileno y fluoruro de hidrógeno se han generado y caracterizado mediante espectroscopía de microondas con transformación de Fourier en haces moleculares. La observación de dos conformeros se debe a la vibración del anillo fuera del plano del sulfuro de trimetileno. Se ha constatado que el conformero axial es el más estable, debido a la existencia de relajación desde el conformero ecuatorial de mayor energía. Esta preferencia conformacional se ha discutido en el contexto del crítico balance existente entre enlaces de hidrógeno primarios y secundarios. La interconversión entre conformeros tiene lugar a través de la vibración del anillo fuera del plano del heterociclo, dado que la barrera para la inversión del anillo se mantiene baja en el complejo como indican los datos experimentales. Los parámetros estructurales del enlace de hidrógeno y del sulfuro de trimetileno se han obtenido del análisis de los espectros de rotación de los isotopómeros  $\text{C}_3\text{H}_6^{32}\text{S} \cdots \text{HF}$ ,  $\text{C}_3\text{H}_6^{34}\text{S} \cdots \text{HF}$ ,  $^{13}\text{C}_\alpha^{12}\text{C}_2\text{H}_6^{32}\text{S} \cdots \text{HF}$  y  $^{13}\text{C}_\beta^{12}\text{C}_2\text{H}_6^{32}\text{S} \cdots \text{HF}$ . Ambos conformeros tienen simetría  $C_s$  con el fluoruro de hidrógeno situado en el plano de simetría del sulfuro de trimetileno que se encuentra plegado un ángulo similar al encontrado en el anillo aislado.

Once the rotational spectrum of the axial conformer was assigned, careful searches allowed the observation of a weaker series of lines spaced  $\approx 4200$  MHz belonging to  $\mu_a$ -type R-branch transitions of the equatorial conformer.

These transitions were approximately seven times less intense than those corresponding to the axial conformer. This seems to indicate that the axial form is the most stable one. Similarly to the axial conformer, some transitions exhibit hyperfine structure due to nuclear spin (H)–nuclear spin (F) coupling. The spectra of  $^{12}\text{C}_3\text{H}_6^{34}\text{S}\cdots\text{HF}$  and  $^{13}\text{C}_\alpha^{12}\text{C}_2\text{H}_6^{32}\text{S}\cdots\text{HF}$  species could also be detected in their natural abundances. All measured frequencies are collected in Table 2.

The spectroscopic constants were determined by fitting a theoretical spectrum calculated from the asymmetric top

Hamiltonian  $\mathbf{H} = \mathbf{H}_\text{R}^{(\text{A})} + \mathbf{H}_\text{ss}$  to the observed frequencies (Tables 1 and 2), using Pickett's program.<sup>[19]</sup>  $\mathbf{H}_\text{R}^{(\text{A})}$  is the A-reduced semirigid rotor Hamiltonian of Watson in the I' representation<sup>[20]</sup> and  $\mathbf{H}_\text{ss} = \mathbf{I}_\text{F} \cdot \mathbf{D} \cdot \mathbf{I}_\text{H}$  is the Hamiltonian for the nuclear spin–nuclear spin interaction,<sup>[21]</sup> where  $\mathbf{D}$  is the nuclear spin(H)–nuclear spin(F) coupling tensor. The total Hamiltonian was set-up in the coupled basis,  $\mathbf{I} = \mathbf{I}_\text{H} + \mathbf{I}_\text{F}$ ,  $\mathbf{F} = \mathbf{I} + \mathbf{J}$ . The derived rotational ( $A$ ,  $B$ ,  $C$ ) and quartic centrifugal distortion constants ( $\Delta_\text{J}$ ,  $\Delta_\text{JK}$ ,  $\Delta_\text{K}$ ,  $\delta_\text{J}$ ,  $\delta_\text{K}$ ) for the axial and equatorial conformers are displayed in Tables 3 and 4, respectively. Only the  $D_\text{aa}$  component of  $\mathbf{D}$  could be determined from the resolved hyperfine components. In all cases, the rms deviation of the fits was commensurate with the estimated accuracy of the frequency measurements.

Table 1. Rotational transitions [MHz] for the axial conformer of trimethylene sulfide  $\cdots$  HF complex.

$J'$	$K'_{-1}$	$K'_{+1}$	$J''$	$K''_{-1}$	$K''_{+1}$	$I'$	$F'$	$I''$	$F''$	$^{12}\text{C}_3\text{H}_6^{32}\text{S}\cdots\text{HF}$		$^{12}\text{C}_3\text{H}_6^{34}\text{S}\cdots\text{HF}$		$^{13}\text{C}_\alpha^{12}\text{C}_2\text{H}_6^{32}\text{S}\cdots\text{HF}$		$^{13}\text{C}_\beta^{12}\text{C}_2\text{H}_6^{32}\text{S}\cdots\text{HF}$	
										obsd	obsd-calcd <sup>[a]</sup>	obsd	obsd-calcd	obsd	obsd-calcd	obsd	obsd-calcd
1	1	1	0	0	0	1	2	1	1	6774.038	−0.005	6667.849	−0.001				
						0	1	0	0	6774.050	0.004						
2	0	2	1	0	1	1	1	1	2	9297.553	−0.001	9245.292	0.000	9232.964	−0.001	9228.130	0.000
2	1	2	1	1	1	1	3	1	2	9070.581	0.002	9002.874	0.008	9020.031	0.008	8989.514	−0.003
						1	2	1	1	9070.539	0.002	9002.823	0.006	9019.977	−0.002		
						0	2	0	1	9070.573	0.002	9002.852	−0.004	9020.011	−0.003		
						1	1	1	1	9070.573	0.002	9002.852	−0.004	9020.011	−0.003		
						1	2	1	2	9070.563	0.006						
						1	1	1	2	9070.596	0.004						
2	1	1	1	1	0	1	3	1	2	9565.349	0.002	9536.835	0.000	9482.158	0.003		
						0	2	0	1	9565.338	0.000	9536.835	0.000	9482.143	−0.003		
						1	1	1	1	9565.338	0.000	9536.835	0.000	9482.143	−0.003		
						1	2	1	1	9565.305	0.001	9536.791	−0.003	9482.114	0.004		
						1	2	1	2	9565.330	0.005						
						1	1	1	0	9565.389	−0.001						
2	0	2	1	1	1	1	3	1	2	7182.591	−0.004						
						0	2	0	1	7182.577	−0.005						
						1	2	1	2	7182.552	0.001						
						1	1	1	1	7182.605	0.006						
2	1	2	1	0	1	1	3	1	2	11185.536	−0.004	11035.691	0.001				
						0	2	0	1	11185.536	−0.004	11035.691	0.001				
						1	2	1	1			11035.713	0.002				
3	0	3	2	0	2	1	4	1	3	13895.755	−0.004	13807.439	−0.001	13804.430	0.003	13784.323	0.000
3	1	3	2	1	2	1	4	1	3	13593.270	−0.002	13489.275	−0.003	13518.795	−0.001	13469.907	0.004
3	1	2	2	1	1	1	4	1	3	14334.231	−0.002	14288.692	0.003	14210.967	−0.006	14254.651	0.000
3	2	2	2	2	1	1	4	1	3	13976.341	0.010						
						1	3	1	2	13976.283	−0.004						
						0	3	0	2	13976.316	−0.004						
3	2	1	2	2	0	1	4	1	3	14057.254	0.006						
						1	3	1	2	14057.206	0.003						
						0	3	0	2	14057.232	−0.006						
3	0	3	2	1	2	1	4	1	3	12007.774	0.000						
						0	3	0	2	12007.764	−0.004						
3	1	3	2	0	2	1	4	1	3	15481.257	0.000	15279.677	0.000				
						0	3	0	2	15481.257	0.000	15279.677	0.000				
						1	2	1	1	15481.243	−0.001	15279.662	0.000				
4	0	4	3	0	3	1	5	1	4	18438.307	−0.001	18304.335	−0.004	18325.946	−0.002	18277.753	0.000
4	1	4	3	1	3	1	5	1	4	18102.306	−0.002	17959.602	−0.005	18005.316	−0.003	17934.833	−0.001
4	1	3	3	1	2	1	5	1	4	19085.092	0.000	19018.645	−0.002	18923.832	0.002		
4	2	3	3	2	2	1	5	1	4	18618.487	−0.004						
4	2	2	3	2	1	1	5	1	4	18815.055	−0.002						
4	2	3	4	1	4	1	5	1	5	7986.351	0.000						
4	0	4	3	1	3	1	5	1	4	16852.812	0.001	16832.104	0.002				
5	0	5	4	0	4	1	6	1	5	22920.095	0.005	22733.099	0.002	22791.943	0.000		
5	1	5	4	1	4	1	6	1	5	22595.370	−0.002	22411.448	0.002	22477.416	0.001		
5	1	4	4	1	3	1	6	1	5	23809.419	0.002	23716.092	0.001				
9	2	7	9	1	8	1	10	1	10	6866.315							

[a] Observed-calculated values from rotational parameters of Table 3.

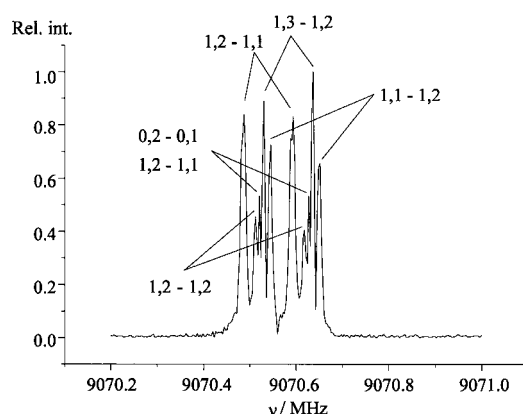


Figure 2.  $2_{1,2} \leftarrow 1_{1,1}$  transition of the axial  $C_3H_6^{32}S \cdots HF$  complex showing the nuclear spin (H)–nuclear spin(F) hyperfine components splitted by Doppler effect.

**Symmetry and structure:** A first insight on the structure of the conformers comes from the observation in the supersonic jet of both axial and equatorial forms which is a compelling evidence that the two nonbonding electron pairs at the S atom are nonequivalent as a consequence of the puckered conformation of the ring.

The values of the planar moments  $P_c = \sum_i m_i c_i^2$  collected in Tables 3 and 4 are practically identical for the parent,  $^{34}S$  and  $^{13}C_\beta$  (axial conformer) isotopic species, which indicates that these atoms are located in the  $ab$  principal inertial plane of each conformer. In addition, this plane coincides with the  $ac$  symmetry plane of bare TMS: the ground vibrational state

value of  $P_b$  in TMS is  $43.98299(16) \text{ u}\text{\AA}^2$  (calculated from ref. [17]), very similar to the  $P_c$  planar moments of both conformers. This is a conclusive evidence that the  $ab$  principal inertial planes of the conformers are also symmetry planes, and that the HF subunit in both conformers is located in them. Therefore, the axial and equatorial conformers of the  $TMS \cdots HF$  complex have  $C_s$  symmetry.

The determination of an  $r_0$ -like structure for each conformer was done by means of iterative least squares fits<sup>[22]</sup> of the rotational constants given in Tables 3 and 4. In this procedure the geometry of the HF monomer<sup>[16]</sup> was assumed to be unaltered upon complexation and the hydrogen atoms of the methylene groups were situated at distances  $r(C-H) = 1.09 \text{ \AA}$  and angles  $\angle HCH = 108^\circ$  with a  $C_{2v}$  local symmetry around the C atoms. Information on the location of the H atom of the HF subunit, and consequently on the deviation from collinearity of the  $S \cdots H-F$  fragment, can be provided by the coupling constant  $D_{aa}$ , which is related to the  $\alpha_{az}$  angle between the  $a$  principal inertial axis and the HF bond ( $z$ ) (see Figure 3) through Equation (1).<sup>[23]</sup>

$$D_{aa} = \frac{1}{4} D_0 \langle 3 \cos^2 \beta - 1 \rangle \langle 3 \cos^2 \alpha_{az} - 1 \rangle \quad (1)$$

where  $D_0$  is the nuclear spin–nuclear spin constant of free HF ( $D_0 = -286.75 \text{ kHz}$ <sup>[24, 25]</sup>) and  $\beta$  is the HF oscillation angle about its centre of mass. This equation allows us to estimate the  $\alpha_{az}$  angle under the assumption of no lengthening of the HF distance once the complex is formed. Taking an average value of  $\beta = 20(5)^\circ$ <sup>[18, 23]</sup> and the quoted errors for  $D_{aa}$ ,  $\alpha_{az}$  angles of  $31.3(26)$  and  $37.5(34)^\circ$  were calculated for the axial and equatorial forms, respectively.

Table 2. Rotational transitions [MHz] for the equatorial conformer of trimethylene sulfide  $\cdots HF$  complex.

$J'$	$K'_{-1}$	$K'_{+1}$	$J''$	$K''_{-1}$	$K''_{+1}$	$I'$	$F'$	$I''$	$F''$	$^{12}C_3H_6^{32}S \cdots HF$		$^{12}C_3H_6^{34}S \cdots HF$		$^{13}C_\alpha^{12}C_2H_6^{32}S \cdots HF$	
										obsd	obsd-calcd <sup>[a]</sup>	obsd	obsd-calcd	obsd	obsd-calcd
1	1	1	0	0	0	1	2	1	1	7254.904	0.002				
2	0	2	1	0	1	1	3	1	2	8387.064	−0.002	8354.144	0.002	8340.476	0.002
2	1	2	1	1	1	1	2	1	1	8304.175	0.002	8457.087	0.002		
							0	2	0	8304.195	−0.004				
							1	3	1	8304.209	0.004				
2	1	1	1	1	0	1	2	1	1	8473.550	−0.002				
							0	2	0	8473.582	0.000				
							1	3	1	8473.582	0.000				
2	1	2	1	0	1	1	3	1	2	11364.618	0.003				
3	0	3	2	0	2	1	4	1	3	12575.833	−0.001	12524.537	0.000	12506.963	0.001
3	1	3	2	1	2	1	3	1	2	12454.859	−0.004			12401.454	−0.001
							1	4	1	12454.874	0.002				
3	1	2	2	1	1	1	4	1	3	12708.750	−0.003	12683.525	−0.001	12621.714	−0.003
3	2	2	2	2	1	1	3	1	2	12583.276	−0.001				
							1	4	1	12583.311	0.002				
3	2	1	2	2	0	1	3	1	2	12590.204	0.004				
							1	4	1	12590.238	0.006				
3	0	3	2	1	2	0	3	0	2	9598.278	−0.001				
							1	4	1	9598.289	0.004				
3	1	3	2	0	2	1	4	1	3	15432.419	−0.002				
4	0	4	3	0	3	1	5	1	4	16758.936	0.002	16687.002	−0.004	16668.983	−0.001
4	1	4	3	1	3	1	5	1	4	16603.857	−0.003	16506.798	0.001		
4	1	3	3	1	2	1	5	1	4	16941.952	−0.004	16907.398	0.000	16826.420	0.001
4	2	3	3	2	2	1	5	1	4	16775.566	−0.006				
4	2	2	3	2	1	1	5	1	4	16792.824	0.001				
5	0	5	4	0	4	1	6	1	5	20934.604	0.004	20839.141	0.002		
5	1	5	4	1	4	1	6	1	5	20750.669	0.000	20628.049	0.000		
5	1	4	4	1	3	1	6	1	5	21172.494	0.000	21127.761	0.000		

[a] Observed-calculated values from rotational parameters of Table 3.

Table 3. Rotational parameters for the axial conformer of trimethylene sulfide...HF complex.

	C <sub>3</sub> H <sub>6</sub> <sup>32</sup> S...HF	C <sub>3</sub> H <sub>6</sub> <sup>34</sup> S...HF	<sup>13</sup> C <sub>α</sub> C <sub>2</sub> H <sub>6</sub> <sup>32</sup> S...HF	<sup>13</sup> C <sub>β</sub> C <sub>2</sub> H <sub>6</sub> <sup>32</sup> S...HF
<i>A</i> [MHz]	4568.2375(27) <sup>[a]</sup>	4483.8759(39)	4512.86(12)	4498.45(20)
<i>B</i> [MHz]	2453.24470(61)	2451.0176(11)	2428.3648(16)	2443.9928(16)
<i>C</i> [MHz]	2205.85439(60)	2184.02296(95)	2197.2931(13)	2181.9194(16)
$\Delta_J$ [kHz]	5.770(11)	5.558(13)	5.745(32)	5.684(70)
$\Delta_{JK}$ [kHz]	14.73(11)	14.71(34)	13.0(11)	14.5(18)
$\Delta_K$ [kHz]	−15.80(78)	[−15.80] <sup>[b]</sup>	[−15.80]	[−15.80]
$\delta_J$ [kHz]	1.0615(89)	1.061(13)	1.037(21)	[1.0615]
$\delta_K$ [kHz]	−6.84(32)	[−6.84]	[−6.84]	[−6.84]
<i>D</i> <sub>aa</sub> [kHz]	−137.3(69)	−155.(13)	−142.(14)	−
<i>N</i> <sup>[c]</sup>	46	26	17	7
<i>J</i> <sub>max</sub>	9	5	5	4
$\sigma^{\text{dof}}$ [kHz]	3.6	3.1	3.3	2.0
<i>P</i> <sub>c</sub> <sup>[e]</sup> [uÅ <sup>2</sup> ]	43.76257(42)	43.75175(48)	45.0504(19)	43.7540(30)

[a] Standard error in parentheses in units of the last digit. [b] Parameters in square brackets were fixed to the corresponding C<sub>3</sub>H<sub>6</sub><sup>32</sup>S...HF value. [c] Number of fitted hyperfine components. [d] rms deviation of the fit. [e]  $P_c = (I_a + I_b - I_c)/2 = \sum_i m_i c_i^2$ . Conversion factor: 505379.1 MHz uÅ<sup>2</sup>.

Table 4. Rotational parameters for the equatorial conformer of trimethylene sulfide...HF complex.

	C <sub>3</sub> H <sub>6</sub> <sup>32</sup> S...HF	C <sub>3</sub> H <sub>6</sub> <sup>34</sup> S...HF	<sup>13</sup> C <sub>α</sub> C <sub>2</sub> H <sub>6</sub> <sup>32</sup> S...HF
<i>A</i> [MHz]	5199.9913(34) <sup>a</sup>	5102.35(44)	5125.6(22)
<i>B</i> [MHz]	2139.6249(11)	2139.4154(17)	2122.2712(18)
<i>C</i> [MHz]	2054.89140(93)	2039.0235(22)	2048.7462(13)
$\Delta_J$ [kHz]	7.344(11)	7.171(17)	7.137(53)
$\Delta_{JK}$ [kHz]	−22.76(11)	[−22.76] <sup>[b]</sup>	[−22.76] <sup>[b]</sup>
$\Delta_K$ [kHz]	[0.0] <sup>[c]</sup>	[0.0] <sup>[c]</sup>	[0.0] <sup>[c]</sup>
$\delta_J$ [kHz]	1.380(13)	1.432(22)	[1.38] <sup>[b]</sup>
$\delta_K$ [kHz]	[0.0] <sup>[c]</sup>	[0.0] <sup>[c]</sup>	[0.0] <sup>[c]</sup>
<i>D</i> <sub>aa</sub> [kHz]	−103.(10)	−	−
<i>N</i> <sup>[d]</sup>	28	10	6
<i>J</i> <sub>max</sub>	5	5	4
$\sigma^{\text{dof}}$ [kHz]	3.0	1.6	1.6
<i>P</i> <sub>c</sub> <sup>[e]</sup> [uÅ <sup>2</sup> ]	43.72437(49)	43.7089(49)	45.026(21)

[a] Standard error in parentheses in units of the last digit. [b] Parameters fixed to the corresponding C<sub>3</sub>H<sub>6</sub><sup>32</sup>S...HF value. [c] Parameters fixed to zero in the fit. [d] Number of fitted hyperfine components. [e] rms deviation of the fit. [f]  $P_c = (I_a + I_b - I_c)/2 = \sum_i m_i c_i^2$ . Conversion factor: 505379.1 MHz uÅ<sup>2</sup>.

Table 5. Experimental structural parameters for axial and equatorial conformers of trimethylene sulphide...HF complex.

Parameters <sup>[a, b]</sup>	TMS...HF Axial	TMS...HF Equatorial
<i>r</i> (S–C <sub>α</sub> ) [Å]	1.833(6) <sup>[c]</sup>	1.833(17)
<i>r</i> (C <sub>α</sub> –C <sub>β</sub> ) [Å]	1.546(7)	1.56(2)
<i>r</i> (C <sub>α</sub> –C <sub>γ</sub> ) [Å]	2.277(5)	2.276(5)
<i>r</i> (F...S) [Å]	3.094(2)	3.067(14)
∠C <sub>α</sub> –S–C <sub>α</sub> [°]	76.8(4)	76.8(9)
∠C <sub>α</sub> –C <sub>β</sub> –S [°]	91.2(3)	91.8(9)
∠C <sub>β</sub> –C <sub>α</sub> –C <sub>β</sub> [°]	94.9(5)	93.6(17)
$\gamma$ [°]	25.4(4)	25.(2)
<i>r</i> (S...H) [Å]	2.17(4)	2.16(6)
$\phi$ [°]	88.82(16)	89.8(3)
$\varphi$ [°]	91.1(15)	93.(3)
$\theta$ [°]	8.(4)	12.(6)
<i>r</i> (X...H <sub>α</sub> ) [Å]		3.09(3)
<i>r</i> (X...H <sub>β</sub> ) [Å]	2.97(2)	

[a] See Figure 3 for notation. [b] The remaining parameters were kept fixed at standard values of *r*(C–H) = 1.09 Å and ∠HCH = 108° (with a C<sub>2v</sub> local symmetry around the C atoms). [c] Standard errors in parentheses in units of the last digit.

The definitive *r*<sub>0</sub>-like structures were determined in final least squares fits constraining the  $\alpha_{\text{az}}$  angles to the above values. The fitted parameters *r*(C<sub>α</sub>–C<sub>β</sub>), *r*(S–C<sub>α</sub>), *r*(S...F), and the angles  $\gamma$  (angle of puckering of the TMS ring) and  $\phi$  (angle between the line bisecting the CSC angle and the S...F internuclear line) are collected in Table 5 along with the derived hydrogen bond parameters *r*(S...H),  $\varphi$  (angle between the S...H hydrogen bond and the line bisecting the CSC angle) and  $\theta$  (angle of deviation of the S...H-F frag-

ment from collinearity). The geometries of both forms, drawn to scale, are shown in Figure 3. These geometries reproduce the experimental rotational constants within 0.5 %.

**Conformational preference and relaxation:** Spectroscopic studies in seeded supersonic jets of noble gases (He, Ne, Ar) have shown that certain conformers, predicted to be among the lowest energy group conformers, are not detected in the adiabatic expansion.<sup>[26]</sup> It has also been reported that this phenomenon is observed when the barrier to interconversion between the conformers is less than about 400 cm<sup>−1</sup>.<sup>[27]</sup> To explain this experimentally observed feature the possibility for certain conformers relaxing to lower energy conformers during the expansion must be considered. Hence, it is accepted that the relaxation is produced by collisions with the inert carrier gas and that this event takes place with more efficiency when a heavier inert gas is used.

With the aim of elucidating the conformational preference and check the behaviour of TMS...HF with respect to relaxation, several tests were carried out diluting ≈1 % of each component in He or Ar at stagnation pressures of about 2 bar. After optimizing conditions, we polarized at the positions of measured  $\mu_a$ -type R-branch transitions of both conformers. Using He as carrier gas the transitions of the equatorial conformer were approximately seven times less intense than those corresponding to the axial conformer (ax:eq ≈ 7:1). Coarse calculations on the electric dipole moments yielded very similar values for the  $\mu_a$  components for both conformers, so the difference in intensity cannot be attributed to a large discrepancy between the dipole moment components. This was a first hint that the axial form is the most stable one. Surprisingly, no sign of the equatorial form was found with Ar even after accumulating more than 8000 shots. Considering the intensity ratio with He and the strength showed by the transitions of the axial conformer in Ar, the corresponding transitions of the equatorial form must have enough intensity to be easily detected in Ar. Thus, we can conclude that relaxation from the equatorial to the axial form occurs in the supersonic expansion during the formation of the TMS...HF, being the axial conformer the most stable one.

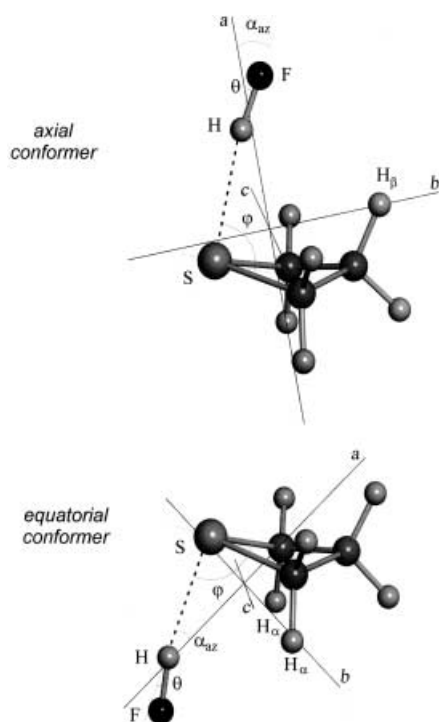


Figure 3. Structures of axial and equatorial conformers of trimethylene sulfide...HF.

## Discussion

The observation of two rotamers in the supersonic expansion proves that TMS...HF complex is a mixture of axial and equatorial conformers. This observation is a consequence of the existence of a ring-puckering large-amplitude motion in the TMS subunit that survives after the hydrogen-bond formation. Hence the double minimum potential function is retained after the interaction with HF, emerging two non-equivalent binding sites at the S atom which result in different axial and equatorial conformers.

The structural parameters of the TMS monomer in the complex,  $r(C_\alpha-C_\beta)$  and  $r(S-C_\alpha)$  distances and the ring-puckering angles  $\gamma$ , have been found to be practically equal for both conformers and they have almost the same values as obtained for TMS in the related heterodimer TMS...HCl.<sup>[15]</sup> Moreover, the values of these ring-puckering angles are very close to that of  $\approx 28^\circ$  derived for free TMS,<sup>[17]</sup> which might indicate a non-significant distortion of TMS configuration upon complexation.

The hydrogen-bond distances  $r(S\cdots H)$  shown in Table 5 are identical for the axial and equatorial conformers and similar to those determined for related complexes thiirane...HF (2.193(18) Å<sup>[18]</sup>), tetrahydrothiophene...HF (2.15(4) Å<sup>[9]</sup>) and pentamethylene sulfide...HF (2.27(1) Å for the axial and 2.18(2) Å for the equatorial).<sup>[5]</sup> Furthermore these distances are slightly shorter than those of 2.28(2) Å and 2.26(6) Å determined for the axial and equatorial conformers of the TMS...HCl complex<sup>[12]</sup> following the same trend observed in other hydrogen-bond complexes when a Cl atom is replaced by a F nucleus.<sup>[5, 6-9]</sup>

The angles  $\varphi$  between the line bisecting the CSC angle and the  $S\cdots H$  (see Figure 3) bond derived for both forms provide evidence of a local  $C_{2v}$  symmetry around the S atom. Moreover, if we accept that the direction of the HF molecule acts as a probe for the orientation of the nonbonding electron pairs at the S atom,<sup>[28]</sup> the axis of these pairs in TMS appears to be perpendicular to the CSC plane. This can be also rationalized considering the HOMO–LUMO model which interprets the new bond as an interaction between the  $\sigma^*$  LUMO of HF and the  $n_\pi$  HOMO orbital of TMS, orthogonal to the S–C bonds. The same conclusion has been reached in the study of TMS...HCl complex.<sup>[12]</sup>

An interesting aspect to examine is the nonlinearity of the hydrogen bonds manifested in the values of the  $\theta$  angles of Table 5. The large quoted errors for the small  $\theta$  values support the existence of nearly linear hydrogen bonds for both conformers. In some related complexes with HX<sup>[4, 7-10, 12, 29-32]</sup> secondary hydrogen bond interactions between the  $X^{\delta-}$  and the nearest methylene hydrogen groups of the ring have been invoked to account for these distortions in the usual linearity of the primary hydrogen bond. Typical distances between the atoms involved in this second-order interaction for HF complexes lie in the range 2.8–3.2 Å.<sup>[3, 7, 9, 11, 18, 23, 30, 33]</sup> In the TMS...HF complex, the  $F^{\delta-}$  could interact with the hydrogen atoms attached to the  $\alpha$ -CH<sub>2</sub> groups of the equatorial conformer or with the hydrogen atom of the  $\beta$ -CH<sub>2</sub> group in the case of the axial form (see Figure 3). The calculated distances of  $r(F\cdots H_\beta) = 2.97(2)$  Å and  $r(F\cdots H_\alpha) = 3.09(3)$  Å (within the reported interval) allow us to infer the existence of secondary hydrogen bonds in the axial and equatorial conformers of the TMS...HF complex.

An interesting point to discuss in the above context is the observed conformational preference. If we accept that the strength of the primary hydrogen bond is connected with the  $S\cdots H$  distance, no conformational preference can be anticipated from the near values of 2.17 and 2.16 Å calculated for the axial and equatorial conformers, respectively. Despite the presence of secondary hydrogen bond interactions in both forms, the shorter value for the  $r(F\cdots H_\beta)$  distance in the axial conformer would explain the relative stability ax:eq  $\approx 7:1$  observed in TMS...HF complex. Same arguments have been used in related complexes.<sup>[5]</sup>

On the basis of the relaxation observed, the barrier to the ring-puckering motion of TMS must be maintained below the limit of  $\approx 400$  cm<sup>-1</sup> after complexation, taking place the interconversion between conformers through the ring inversion of TMS. This behaviour is consistent with that previously reported for TMS...HCl<sup>[12]</sup> and with the fact that no relaxation in the related pentamethylene sulfide...HCl and HF complexes was observed.<sup>[4, 5]</sup> In pentamethylene sulfide the barrier to invert the ring configuration has been reported to be 4057 cm<sup>-1</sup>.<sup>[34]</sup> Fortunately here a relatively high barrier for interconversion between the conformers exists which leads to an incomplete vibrational relaxation in the jet-cooled beam of the experiment. Thus, both axial and equatorial rotamers get trapped within their respective individual wells of the asymmetric potential function (see Figure 1d) so they are observable in a very low-temperature experiment using He as carrier gas.

## Experimental Section

The rotational spectrum of TMS...HF dimer was investigated in the 5–26 GHz region using the MB-FTMW spectrometer described elsewhere,<sup>[35]</sup> so only essential details need to be given here. The trimethylene sulfide...hydrogen fluoride complex was generated through the adiabatic expansion in a evacuated chamber of gas mixtures of  $\approx 1\%$  of each component in He at backing pressures of  $\approx 2$  bar. Microwave pulses of  $0.2\ \mu\text{s}$  at 40 mW excitation powers were coupled in a Fabry–Perot cavity formed of two aluminium mirrors arranged coaxially and near confocally. In the centre of one mirror is located a solenoid nozzle which was used to generate molecular pulses of 0.28–0.36 ms along the cavity axis. If the radiation interacts with the sample the subsequent emission is detected in the time domain, digitised and Fourier transformed to produce a frequency domain spectrum. Since the molecular beam travels parallel to the microwave radiation, every line is split into two components due to the Doppler effect. The resonance frequency is then calculated as the arithmetic mean of the Doppler components. The accuracy of frequency measurements is estimated to be better than 5 kHz.

## Acknowledgement

The authors wish to thank the Ministerio de Ciencia y Tecnología (DGI Grant BQU2000-0869) the Junta de Castilla y León (Grants VA41/00B and VA017/01) and the Fundación Ramon Areces for financial support. M.E.S. gratefully acknowledges an FPI grant from the Ministerio de Educación y Cultura.

- 
- [1] T. J. Balle, W. H. Flygare, *Rev. Sci. Instrum.* **1981**, 52, 33–45.  
[2] S. Antolínez, J. C. López, J. L. Alonso, *Angew. Chem.* **1999**, 111, 1889–1891; *Angew. Chem. Int. Ed.* **1999**, 38, 1772–1774.  
[3] S. Antolínez, J. C. López, J. L. Alonso, *ChemPhysChem* **2001**, 2, 114–117.  
[4] M. E. Sanz, J. C. López, J. L. Alonso, *Chem. Eur. J.* **1999**, 5, 3293–3298.  
[5] S. Blanco, A. Lesarri, J. C. López, J. L. Alonso, *Chem. Eur. J.* **2002**, 8, 1603–1613.  
[6] J. C. López, J. L. Alonso, F. J. Lorenzo, V. M. Rayón, J. A. Sordo, *J. Chem. Phys.* **1999**, 111, 6363–6374.  
[7] J. L. Alonso, J. C. López, S. Blanco, A. Lesarri, F. J. Lorenzo, *J. Chem. Phys.* **2000**, 113, 2760–2767.  
[8] M. E. Sanz, J. C. López, J. L. Alonso, *J. Phys. Chem. A* **1998**, 102, 3681–3689.  
[9] M. E. Sanz, J. C. López, J. L. Alonso, *Chem. Phys. Lett.* **1998**, 288, 760–766.  
[10] S. Antolínez, J. C. López, J. L. Alonso, *Chem. Phys. Lett.* **2001**, 334, 250–256.  
[11] M. E. Sanz, V. M. Sanz, J. C. López, J. L. Alonso, *Chem. Phys. Lett.* **2001**, 342, 31–38.  
[12] M. E. Sanz, J. C. López, J. L. Alonso, *Angew. Chem.* **2001**, 113, 961–964; *Angew. Chem. Int. Ed.* **2001**, 40, 935–938.  
[13] A. Lesarri, S. Blanco, J. C. López, *J. Mol. Struct.* **1995**, 354, 237–243 and references therein.  
[14] D. O. Harris, H. W. Harrington, A. C. Luntz, W. D. Gwinn, *J. Chem. Phys.* **1966**, 44, 3467–3480.  
[15] J. C. López, A. G. Lesarri, J. L. Alonso, R. Spiehl, A. Guarnieri, *Mol. Phys.* **1994**, 82, 283–302.  
[16] G. Guelachvili, *Opt. Commun.* **1976**, 19, 150–154.  
[17] R. Hinze, A. Guarnieri, J. L. Alonso, J. C. López, *J. Mol. Struct.* **1995**, 350, 195–204.  
[18] M. J. Atkins, A. C. Legon, H. E. Warner, *Chem. Phys. Lett.* **1994**, 229, 267–272.  
[19] H. M. Pickett, *J. Mol. Spectrosc.* **1991**, 148, 371–377.  
[20] J. K. G. Watson in *Vibrational Spectra and Structure*, Vol. 6 (Ed.: J. R. Durig), Elsevier, Amsterdam, **1977**, pp. 1–89.  
[21] W. G. Read, W. H. Flygare, *J. Chem. Phys.* **1982**, 76, 2238–2246.  
[22] H. D. Rudolph, *Struct. Chem.* **1991**, 2, 581–588.  
[23] A. C. Legon, A. L. Wallwork, D. J. Millen, *Chem. Phys. Lett.* **1991**, 178, 279–284.  
[24] J. S. Muentner, W. Klemperer, *J. Chem. Phys.* **1970**, 52, 6033–6037.  
[25] J. S. Muentner, *J. Chem. Phys.* **1972**, 56, 5409–5412.  
[26] P. D. Godfrey, R. D. Brown, F. M. Rodgers, *J. Mol. Struct.* **1996**, 376, 65–81.  
[27] R. S. Ruoff, T. D. Klots, T. Emilsson, H. S. Gutowsky, *J. Chem. Phys.* **1990**, 93, 3142–3150.  
[28] A. C. Legon, D. J. Millen, *Chem. Soc. Rev.* **1987**, 16, 467–498.  
[29] A. C. Legon, *Faraday Discuss.* **1994**, 97, 19–.  
[30] J. Cosléou, D. G. Lister, A. C. Legon, *Chem. Phys. Lett.* **1994**, 231, 151–158.  
[31] S. Antolínez, A. Lesarri, J. C. López, J. L. Alonso, *Chem. Eur. J.* **2000**, 6, 3345–3350.  
[32] S. Antolínez, J. C. López, J. L. Alonso, *Chem. Phys. Lett.* **2000**, 323, 130–136.  
[33] S. Antolínez, M. Gerbi, J. C. López, J. L. Alonso, *Phys. Chem. Chem. Phys.* **2001**, 3, 796–799.  
[34] J. B. Lambert, R. G. Keske, D. K. Weary, *J. Am. Chem. Soc.* **1967**, 89, 5921–5924.  
[35] J. L. Alonso, F. J. Lorenzo, J. C. López, A. Lesarri, S. Mata, H. Dreizler, *Chem. Phys.* **1997**, 218, 267–275.

Received: February 20, 2002 [F 3890]